Rapid and simple ^{13}C-hyperpolarization by ^{1}H dissolution dynamic nuclear polarization followed by an in-line magnetic field inversion

Quentin Stern,[1†] Quentin Reynard-Feytis,[1] Stuart J. Elliott,[1,2] Morgan Ceillier,[1] Olivier Cala,[1] Konstantin Ivanov,[3] and Sami Jannin[1]

[1] *Université Claude Bernard Lyon 1, CRMN UMR-5082, CNRS, ENS Lyon, Villeurbanne 69100 France*

[2] *Molecular Sciences Research Hub, Imperial College London, London W12 0BZ, United Kingdom*

[3] *International Tomography Center, Siberian Branch of the Russian Academy of Science, Novosibirsk, 630090, Russia; Novosibirsk State University, Novosibirsk, 630090, Russia*

[†] *Correspondance: quentin.stern@protonmail.com*

Abstract

Dissolution dynamic nuclear polarization (dDNP) is a method of choice for preparing hyperpolarized ^{13}C metabolites such as 1-^{13}C-pyruvate used for *in vivo* applications including the real-time monitoring of cancer cell metabolism in human patients. The approach consists of transferring the high polarization of electron spins to nuclear spins *via* microwave irradiation at low temperatures (1.0-1.5 K) and moderate magnetic fields (3.3-7 T). The solid sample is then dissolved and transferred to an NMR spectrometer or MRI scanner for detection in the liquid state. Common dDNP protocols use direct hyperpolarization of ^{13}C spins reaching polarizations of >50% in ~1-2 hours. Alternatively, ^{1}H spins are polarized before transferring their polarization to ^{13}C spins using cross-polarization (CP), reaching similar polarization levels as direct DNP in only ~20 min. However, it relies on more complex instrumentation, requiring highly skilled personnel. Here, we explore an alternative route using ^{1}H dDNP followed by an inline adiabatic magnetic field inversion in the liquid state during the transfer. ^{1}H polarizations of >70% in the solid-state are obtained in ~5-10 min. As the hyperpolarized sample travels from the dDNP polarizer to the NMR spectrometer, it goes through a field inversion chamber, which causes ^{1}H→^{13}C polarization transfer. This transfer is made possible by the *J*-coupling between the heteronuclei, which mixes the Zeeman states at zero-field and causes an anti-level crossing. We report liquid-state ^{13}C polarization up to ~17% for 3-^{13}C-pyruvate and ^{13}C-formate. The instrumentation needed to perform this experiment in addition to a conventional dDNP polarizer is simple and readily assembled.

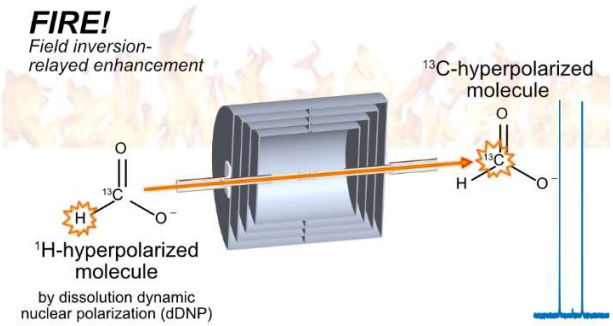

Graphical absract

Introduction

Small molecules with hyperpolarized ^{13}C nuclear spins[1] represent probes with exquisite chemical and spatial resolutions for real-time *in vivo* magnetic resonance imaging (MRI).[2,3] The most important example is [1-^{13}C]-pyruvate, which has been used to detect and monitor the development of prostate cancer in human patients, from an early stage[4]. In addition to medical imaging, hyperpolarization of nuclear spins in the liquid state has also found applications in nuclear magnetic resonance (NMR) spectroscopy,[5] from drug discovery[6,7] and biomolecular NMR[8,9] to chemical reaction monitoring.[10,11] Dissolution dynamic nuclear polarization (dDNP) is a capable of polarizing a large number of molecules reaching polarizations of tens of percent, near the absolute theoretical maximum.[12] The method consists of transferring the high polarization of unpaired electron spins to the surrounding nuclear spins in the solid state using microwave irradiation (μw) at low temperatures (typically 1-2 K) and moderate magnetic fields (typically 3-7 T); once the sample is hyperpolarized, it is dissolved by a burst of hot solvent and transferred to an MRI scanner or NMR spectrometer for use in the liquid state.[13] The most widespread dDNP approach uses the narrow-line radical trityl to transfer the electron spin polarization directly to the ^{13}C spins.[14,15] This allows the ^{13}C spins to polarize to high levels exceeding 60%, but has the disadvantage of being relatively slow, as the sample typically takes 1–2 hours to reach the DNP equilibrium. The throughput of dDNP can be increased by using the broad-line radical TEMPOL to polarize ^{1}H spins and subsequently transfer the polarization from ^{1}H to ^{13}C spins before dissolution in the solid state, using cross-polarization (CP) in Hartman-Hahn conditions (HH-CP)[16–18] or through the dipolar order (dCP).[19,20] The CP-based approach is also capable of reaching high ^{13}C polarization exceeding 60%, but in a much-reduced time of typically 15-20 min. However, the HH-CP approach also has its Achilles heel as it requires strong radiofrequency (rf) powers that are difficult to realize in super-fluidic helium, without detrimental arcing of the NMR coil.

In the past years, spin dynamics in the liquid state at zero to ultra-low field (ZULF) have been abundantly used to transfer spin order from ^{1}H to ^{13}C in parahydrogen-induced polarization experiments (PHIP).[1,21–26] In the context of dDNP experiments, the consequences of spin dynamics at low field have been attested during the transfer of hyperpolarized solution from the polarizer to the liquid-state spectrometer but, to date, they have not been exploited actively to transfer polarization from ^{1}H to ^{13}C spins.[27,28] Here, we propose to prepare ^{13}C-hyperpolarized metabolites using ^{1}H DNP – which can readily be performed within minutes on any existing dDNP device –, followed by dissolution and an inline flow through an adiabatic magnetic field inversion chamber to transfer the ^{1}H Zeeman order to the ^{13}C spins through the *J*-coupling. This inversion chamber might have the potential to become a broadly compatible add-on to any existing dDNP device. We dub this method "field inversion relayed enhancement-dDNP" (FIRE-dDNP). The experimental setup is depicted in Figure 1A-B. The only difference between this experimental setup and standard dDNP setups is the presence of an inversion chamber consisting of commercial mu-metal shields equipped with solenoid coils on 3D printed supports and powered by standard laboratory power supplies. Fig. 1C shows the magnetic field profile of the inversion chamber and the simulated ^{1}H and ^{13}C polarizations as the spins travel through the field profile. The polarization transfer occurs in the region where the magnetic field is in μT range, that is, when the *J* coupling becomes larger than the Zeeman interaction. We present a comprehensive theory of polarization transfers by FIRE. We then demonstrate polarizations up to 17% in the liquid state after only 10 min of DNP for ^{13}C-formate and [3-^{13}C]-pyruvate in DNP juice doped with 50 mM TEMPOL. Finally, we propose routes to extend the applicability of the method to molecules with weak *J* couplings such as [1-^{13}C]-pyruvate, which is highly relevant to *in vivo* imaging.

Theory

FIRE makes use of an adiabatic magnetic field inversion to transfer Zeeman order between heteronuclear spins *via* their *J* coupling. A quantum adiabatic process is a transformation that is slow enough to allow the system to remain in its eigenstates. We first show that an adiabatic field inversion for isolated ^{13}CH and $^{13}CH_3$ spin systems

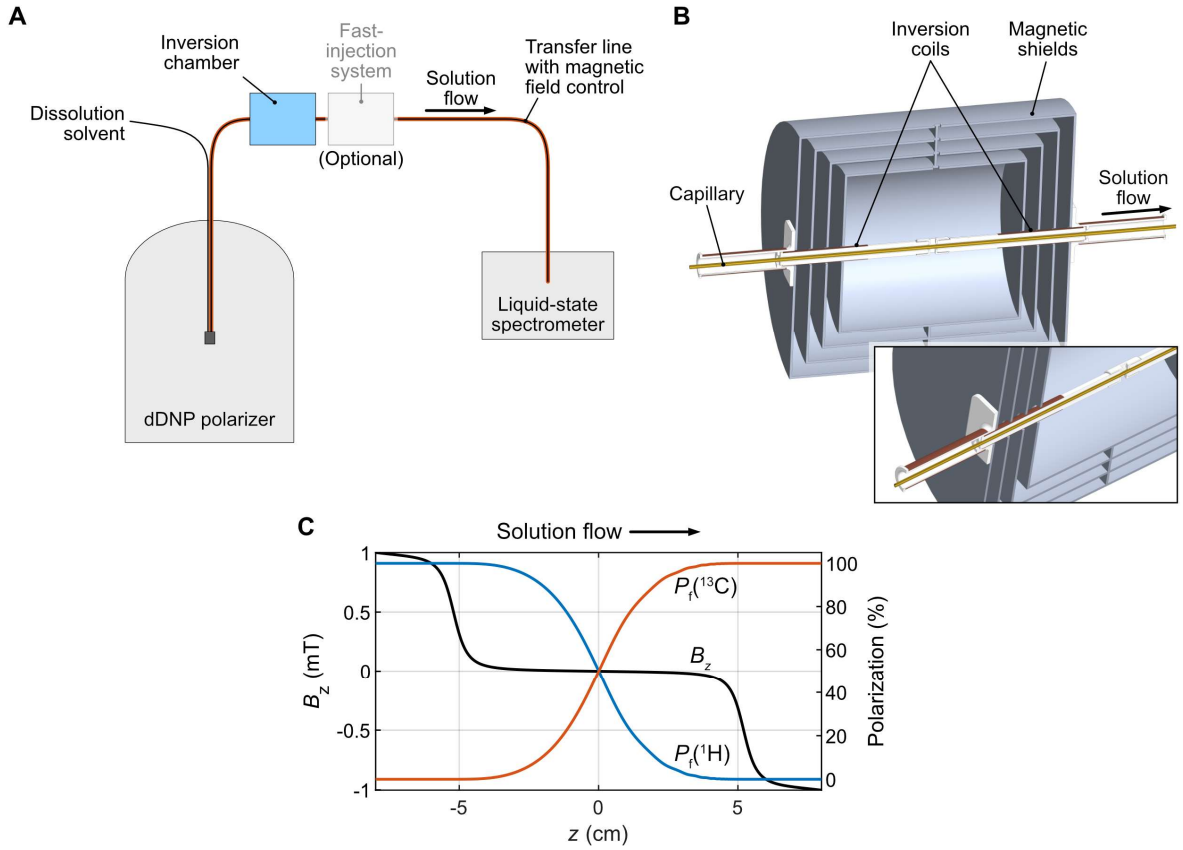

Figure 1: (a) Experimental setup for ^{13}C hyperpolarization by ^1H dDNP followed by FIRE. The inversion chamber is added along the transfer line from the polarizer to the liquid-state spectrometer. As molecules travel through the inversion chamber, polarization transfers from ^1H to ^{13}C spins. (b) 3D cut plane of the inversion chamber. (c) Field profile in the inversion chamber (black line) and simulated ^1H and ^{13}C polarizations along space (colored lines) for ^{13}C-formate, traveling at 4 m.s^{-1}. See the theory section and the Supplementary Material for more details on the simulation.

where ^{13}C and H are *J*-coupled heteronuclear spins, allows ^{13}C and ^1H to exchange polarization. These two model systems correspond to ^{13}C-formate and the three isotopomers of pyruvate with a single ^{13}C label. Note that our approach applies for any CH_n spin system and that the codes provided in the Supplementary Material can generate the analytical solutions for any $n \geq 1$.

The Hamiltonian describing the spin system during the field inversion is the sum

$$\hat{H}_{\text{tot}}(t) = \hat{H}_{\text{Z}}(t) + \hat{H}_J \qquad \text{Eq. 1}$$

of the time-dependent Zeeman Hamiltonian

$$\hat{H}_{\text{Z}}(t) = -B_z(t)\left(\gamma_{\text{S}}\hat{S}_z + \gamma_{\text{I}}\sum_{i=1}^{n}\hat{I}_{iz}\right) \qquad \text{Eq. 2}$$

and the time-independent *J* coupling Hamiltonian

$$\hat{H}_J = J_{\text{IS}}\hat{\boldsymbol{S}}\cdot\sum_{i=1}^{n}\hat{\boldsymbol{I}}_i + J_{\text{II}}\sum_{i>j}^{n}\hat{\boldsymbol{I}}_i\cdot\hat{\boldsymbol{I}}_j, \qquad \text{Eq. 3}$$

where S and I represent ^{13}C and ^{1}H spins, respectively, and $B_z(t)$, γ_I, γ_S, J_{IS}, and J_{II} are the magnetic field intensity along the z axis at time t, the gyromagnetic ratio of I and S spins, and the J coupling between I and S spins and between I spins, respectively. Figure 2 shows the eigenfrequencies of the Hamiltonian as a function of the magnetic field intensity in the case of a ^{13}CH spin system with and without including the J-Hamiltonian (panels B and A, respectively). When the magnetic field is sufficiently strong, the eigenfrequencies vary linearly with the field intensity, *i.e.*, the eigenbasis is given by the Zeeman states. When the field intensity is sufficiently low, the J interaction mixes the $|\alpha\beta\rangle$ and $|\beta\alpha\rangle$ states and causes an avoided crossing or level anticrossing (LAC).[29]

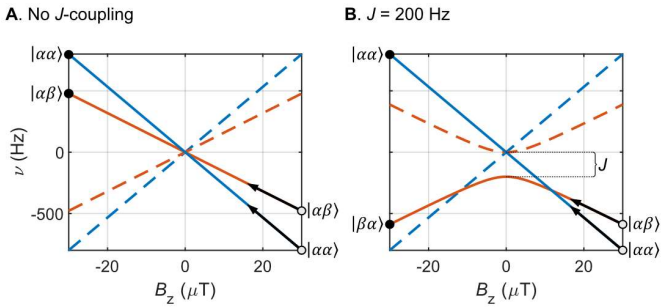

Figure 2: Eigenvalue plots for a pair of ^{1}H and ^{13}C spins without and with a J-coupling of 200 Hz (panels A and B, respectively). The solid and dashed lines represent states that are and are not populated, respectively, assuming initial polarizations $P_i(^{13}C) = 0$ and $P_i(^{1}H) = 1$ and an adiabatic process. The white and black dots represent the initial and final populations, respectively. The black arrows indicate the time evolution of the eigenvalues during the adiabatic field inversion.

If the initial polarizations of ^{1}H and ^{13}C spins are $P_i(^{1}H) = 1$ and $P_i(^{13}C) = 0$, respectively, the population coefficients of states $|\alpha\beta\rangle$ and $|\alpha\alpha\rangle$ are ½, while the other two states are not populated. According to the definition of adiabatic transformations, an adiabatic field inversion causes the states to follow the line represented in Fig. 2. In the absence of a J coupling, Fig. 2 shows that, after inversion, the populations remain on the $|\alpha\beta\rangle$ and $|\alpha\alpha\rangle$ states, that is, no polarization occurs. On the contrary, with a J coupling, the system has populations $|\beta\alpha\rangle$ and $|\alpha\alpha\rangle$ with coefficients ½, after inversion, which corresponds to final polarizations $P_f(^{1}H) = 0$ and $P_f(^{13}C) = 1$. In other words, the polarization of the ^{1}H spin is transferred to spin ^{13}C. In the more general case where ^{1}H spins have any polarization $P_i(^{1}H)$ and ^{13}C spins are not polarized in the initial state, the final polarizations are

$$\begin{aligned} P_f(^{1}\mathrm{H}) &= 0 \\ P_f(^{13}\mathrm{C}) &= P_i(^{1}\mathrm{H}) \end{aligned}. \qquad \text{Eq. 4}$$

In the case of a $^{13}CH_3$ spin system, the same argument can be used to find out the final polarizations from the initial polarizations $P_i(^{1}H)$ and $P_i(^{13}C) = 0$, but the analysis is more complicated as the eigenbasis contains 16 states. We show in the Supplementary Material that the final polarizations are

$$\begin{aligned} P_f(^{1}\mathrm{H}) &= \frac{1}{12}\left(7P_i(^{1}\mathrm{H}) + P_i(^{1}\mathrm{H})^3\right) \\ P_f(^{13}\mathrm{C}) &= \frac{1}{4}\left(5P_i(^{1}\mathrm{H}) - P_i(^{1}\mathrm{H})^3\right) \end{aligned}. \qquad \text{Eq. 5}$$

These analytical expressions are plotted in Fig. S3. To reach this result, we assumed that there are no avoided crossings between states of different total angular momentum.[30] We further assumed that there are no allowed crossings between states of similar total angular momentum and verify the validity of this assumption by visual inspection of the eigenvalue plot (see Fig. S2). Eq. 5 shows that ^{1}H spins, which outnumber ^{13}C spins, do not lose all their polarization as they transfer some of it to ^{13}C spins. In the limit of weak initial ^{1}H polarization (*i.e.*, $|P_i(^{1}H)| \ll 1$), Eq. 5 also shows that the final polarization of I spins is $P_f(^{13}C) = 5P_i(^{1}H)/4$, i.e., the final polarization of ^{13}C spins is ¼ higher than the initial polarization of ^{1}H spins. It should be noted that polarization is defined

with respect to the axis *before* field inversion. As a consequence, the field inversion inverts the sign of polarization if the reference frame is chosen according to the direction of the magnetic field after inversion.

The analysis presented above gives the final polarizations if the field inversion is "infinitely slow" or "sufficiently slow". Landau-Zener theory predicts that the inversion time should be long compared to the inverse of the interaction strength of the perturbation (here, the *J*-coupling) for the transformation to be adiabatic.[31] This means that the inversion time t_{inv} should be longer than $1/J_{IS}$. In the case of ^{13}C-formate, [3-^{13}C]-pyruvate, [2-^{13}C]-pyruvate, and [1-^{13}C]-pyruvate (which have *J* coupling constants of 195, 125, 6.2, and 1.3 Hz) this represents inversion times of approx. 5, 8, 160 and 770 ms, respectively. If the inversion time is of the order of tens of ms, it is therefore expected that ^{13}C-formate and [3-^{13}C]-pyruvate experience an adiabatic process and polarization is efficiently transferred from ^{1}H to ^{13}C spins. On the contrary, for [2-^{13}C]-pyruvate and [1-^{13}C]-pyruvate, the adiabaticity criterion is not fulfilled and the final polarization of ^{13}C spins is close to 0 after the field inversion. The polarizations of ^{1}H and ^{13}C spins after inversion can be predicted more precisely by numerical simulation. The polarization transfer was simulated for four molecules that experience the field profile used in the experiments presented below (shown in Fig. 1C). Initial polarizations of 1 and 0 were assumed for ^{1}H and ^{13}C spins, respectively. Figure 3 shows the numerically-simulated final polarizations of ^{1}H and ^{13}C spins as a function of the inversion time (note that each point on the *x* axis in Fig. 3 corresponds to a different simulated experiment; the curves correspond to the polarizations at the end of an experiment rather than along a single experiment). ^{13}C-formate being a ^{13}CH spin system, Fig. 3 shows that for sufficient inversion time, ^{1}H and ^{13}C spins have polarizations 0 and 1, respectively, in agreement with Eq. 4. [3-^{13}C]-pyruvate being a ^{13}CH$_3$ spin system, Fig. 3 shows that for sufficient inversion time, ^{1}H and ^{13}C spins have polarizations 2/3 and 1, respectively, in agreement with Eq. 5. For [2-^{13}C]-pyruvate and [1-^{13}C]-pyruvate, all simulated experiments have too short inversion times to allow for a significant polarization transfer between ^{1}H and ^{13}C spins. In our experimental setup, the hyperpolarized solution travels at ~4 m.s^{-1}, which represents an inversion time of 40 ms. The simulations in Fig. 3 therefore show that FIRE in these particular conditions should be efficient for ^{13}C-formate and [3-^{13}C]-pyruvate but not for [2-^{13}C]-pyruvate and [1-^{13}C]-pyruvate.

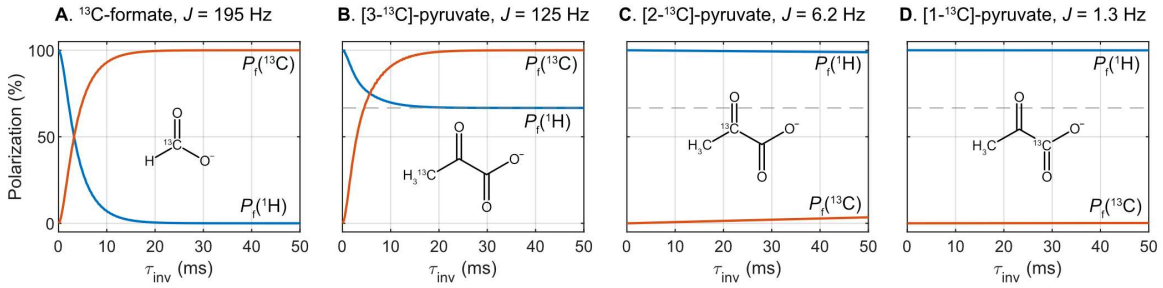

Figure 3: Numerical simulation of the final ^{1}H and ^{13}C polarizations after field inversion, as a function of the inversion time. The simulation assumes that the initial polarizations of the ^{13}C and ^{1}H spins are 0 and 1, respectively.

Results and Discussion

All experiments were performed on a mixture of ^{13}C-formate, [3-^{13}C]-pyruvate, [2-^{13}C]-pyruvate, and [1-^{13}C]-pyruvate (at concentrations of 0.43, 0.44, 0.44, and 0.45 M, respectively) in the glass-forming mixture "DNP juice" (1:3:6 H_2O:D_2O:glycerol-d_8 v/v/v) doped with 50 mM TEMPOL. A single stock solution was prepared and stored in aliquots of 100 µL at –80 °C. For all experiments, 100 µL of the solution was loaded in a PEEK sample cup and rapidly immersed into the liquid helium bath of the cryostat of a 7.05 T dDNP polarizer (*Bruker Biospin* prototype polarizer) to ensure that the sample froze as a homogeneous glass. ^{1}H spins were hyperpolarized under positive DNP using a microwave frequency of 197.648 GHz modulated at a rate of 500 Hz over a bandwidth of 128 MHz (with saw-tooth modulation). Figure 3A shows an example of DNP build-up for this sample at 1.2 K in the solid state monitored every 5 s with a train of 64 pulses of 0.1° nutation angle.[13] The

mean polarization at the end of the DNP build-up for the seven measured samples is 52% with a standard deviation of 2% between samples. Note that the polarization is strongly underestimated due to severe radiation damping (leading to strong line broadening and signal losses during spectrometer dead-time) and is probably closer to 70% at DNP equilibrium (more details on polarization quantification are given in the Supplementary Material).[32] After the ^{1}H polarization plateaued, the sample was dissolved and transferred to a liquid-state 1.88 T benchtop spectrometer (Fourier 80, *Bruker Biospin*) using a fast dissolution, transfer, and injection system, as described elsewhere.[33] The total time between triggering the dissolution process and the sample being injected into the NMR tube was of 1.78 and 1.55 s with and without the inversion chamber along the transfer line. Fig. 3B shows the decay of ^{1}H polarization of the four analytes in the liquid state monitored with 1° pulses every second, in the case where the spins did not experience field inversion, that is, for a standard dDNP experiment. The first spectrum was acquired 1 s after injection. The ^{1}H polarization for ^{13}C-formate and [3-^{13}C]-pyruvate at injection were extrapolated by a mono-exponential fit and were found to be 13.3% ± 0.6% and 12.0% ± 0.1%, respectively. That of [1-^{13}C]-pyruvate and [2-^{13}C]-pyruvate were averaged between the two molecules because their signals are not resolved and is of 11.61% ± 0.06% at injection (see below). The error bars are errors on the fit (see the Supplementary Material for details on the propagation of uncertainty). The loss of polarization during the dissolution and transfer process from ~52% and ~12% can be attributed to paramagnetic relaxation due to the presence of the polarizing agent TEMPOL, in particular at low field in the transfer line between the polarizer and the liquid-state spectrometer (~4 mT).[27] An additional source of relaxation for the three isotopomers of pyruvate is intramolecular dipole-dipole relaxation between the ^{1}H spins, which is likely to be responsible for the lower liquid-state polarizations of pyruvate with respect to that of ^{13}C-formate.[13]

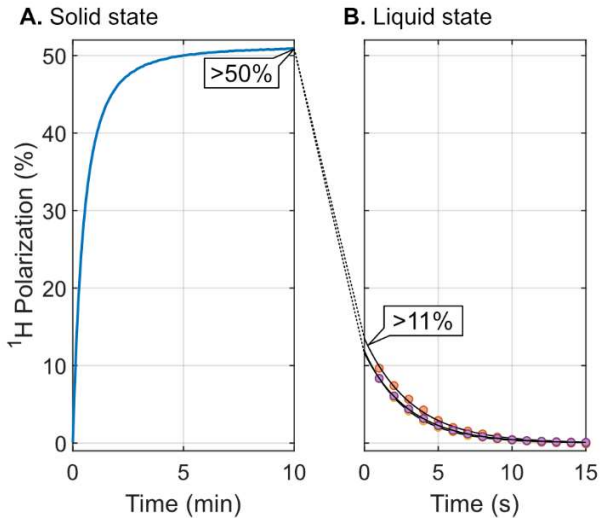

Figure 4: (a) ^{1}H polarization building up under DNP in the solid state at 1.2 K and 7.05 T, reaching 50% after 5 min. (b) Decay of ^{1}H polarization in the liquid state at 1.88 T and XXX K as a function of time after injection without going through the inversion chamber. The experimental data (colored dots) are fitted with a mono-exponential decay (black lines).

The experiment was repeated adding the field inversion chamber along the transfer line between the polarizer and the fast injection system, as shown in Fig. 1. The inversion chamber consists of mu-metal magnetic shields (MS-1, *Twinleaf LLC*) equipped with home-made coils on 3D-printed supports (details on the coils are available in the Supplementary Material). It was located as close as possible to the polarizer to mitigate ^{1}H relaxation before the polarization transfer. ^{1}H spins were hyperpolarized as in the experiment presented in Fig. 4. Before the sample was dissolved, a train of 30 $\pi/2$ pulses was applied to the ^{13}C spins to wipe out their polarization and ensure that the polarization observed in the liquid state did not originate from direct ^{13}C DNP in the solid state. The dissolution process was then carried out as in the experiment presented in Fig. 4. The experiment was repeated twice. In the first case (run #1), ^{13}C spectra were recorded using 5° pulses and a repetition delay of 10 s

starting immediately after injection. In the second case (run #2), a single ^{1}H spectrum was recorded 3 s after injection using a 5° pulse, and only then a series of ^{13}C spectra were recorded using 5° pulses and a repetition delay of 10 s. In the latter case, the first ^{13}C spectrum was recorded ~7 s after injection (this delay is approximate because the time for the NMR control system *Topspin* to launch the ^{13}C pseudo-2D experiment following the 1D ^{1}H spectrum is not well defined). Figure 5A shows the first hyperpolarized ^{13}C spectrum of run #1. As expected from our theoretical predictions, ^{13}C-formate and [3-^{13}C]-pyruvate yield strong signals while [1-^{13}C]-pyruvate is barely detectable (polarization of ~0.3%). Unfortunately, the spectral window was too narrow to detect [2-^{13}C]-pyruvate (this is the case for all ^{13}C-detected experiments). Fig. 5B shows the decay of ^{13}C polarization for ^{13}C-formate and [3-^{13}C]-pyruvate in run #2. Mono-exponential fits were used to extrapolate the polarization at the time of injection (see Eq. S31). We performed two additional ^{13}C-detected experiments without field inversion as negative experiments. In the first case (run #3), the solution traveled through the inversion chamber, but the polarity of the solenoids was changed so that the magnetic field did not invert. As a consequence, the spins experienced a region of low field in the μT region but no actual field inversion. In the second case (run #4), the inversion chamber was removed from the transfer line. Again, a single ^{1}H spectrum was recorded with a 1° pulse 3 s after injection and then the decay of ^{13}C polarization was recorded with 5° pulses every 10 s. In both cases, the ^{13}C polarization yielded non-negligible values at injection on the order of 2% and 6% for ^{13}C-formate and [3-^{13}C]-pyruvate, respectively. Fig 5C and Table 1 summarize the polarization values at the time of injection (note that for experiments #2, #3, and #4, this value is an extrapolation).

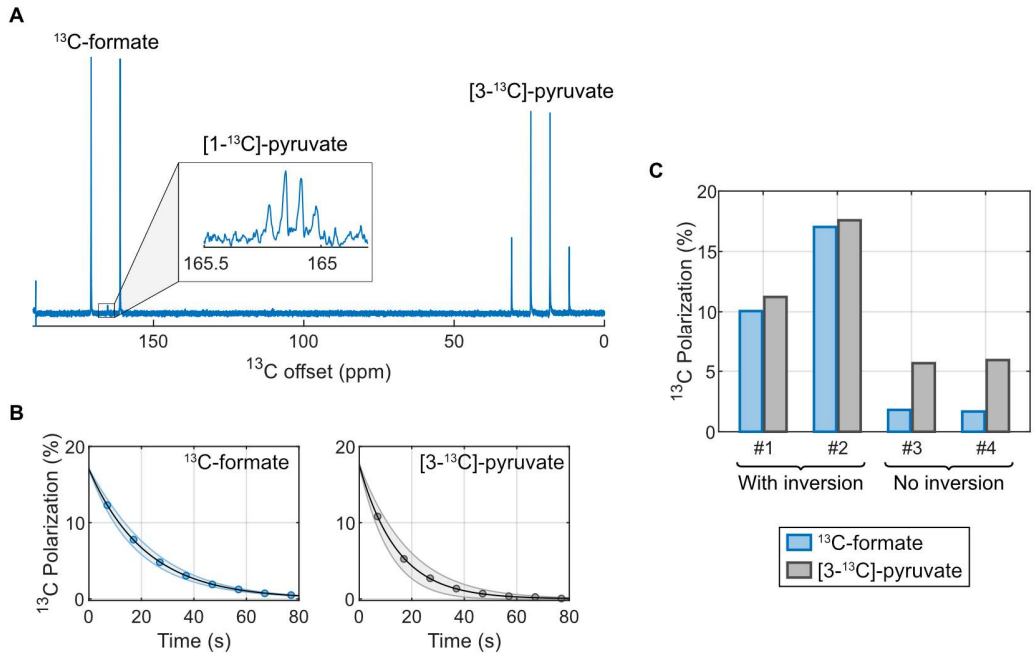

Figure 5: (a) Hyperpolarized ^{13}C signal after inversion in the liquid state for ^{13}C-formate and 3-^{13}C-pyruvate at 1.88 T. The inlet shows the weak signal originating from 1-^{13}C-pyruvate (b) Decays of ^{13}C polarization monitored with 5° pulses for ^{13}C-formate and 3-^{13}C-pyruvate as a function of time after injection in the case where the spin experienced a field inversion during the sample transfer. The colored areas around the fitted curves represent the predicted polarization with 95% confidence. (c) Comparison of the ^{13}C polarization at the time of injection in the liquid state for the four ^{13}C-detected experimental runs. See the text for experimental details on the different runs.

Table 1: ^{13}C longitudinal relaxation time constants in s and polarizations in % at the time of injection obtained by mono-exponential fits of the decaying hyperpolarized signals recorded using 5° pulses. The error bars correspond to errors on the fit (which do not include the uncertainty on signal integrals).

Experiment		^{13}C-formate		[3-^{13}C]-pyruvate		[1-^{13}C]-pyruvate	
		T_1(^{13}C)	P(^{13}C)	T_1(^{13}C)	P(^{13}C)	T_1(^{13}C)	P(^{13}C)
With inversion	#1	21.3 ± 0.3	10.06 ± 0.09	14.0 ± 0.2	11.23 ± 0.08	82 ± 9	0.3 ± 0.02
	#2	21.7 ± 0.2	17.0 ± 0.1	14.4 ± 0.3	17.6 ± 0.3	106 ± 15	0.3 ± 0.02
No inversion	#3	29 ± 4	1.8 ± 0.2	16.1 ± 0.9	5.7 ± 0.3	69 ± 98	0.02 ± 0.02
	#4	28 ± 2	1.7 ± 0.1	15.5 ± 0.8	5.9 ± 0.3	101 ± 23	0.13 ± 0.02

The lower performance in run #1 compared with run #2 (where the experimental process was exactly the same except for the detection scheme in the liquid state) is surprising but might simply come from a lack of repeatability from the operator during the dissolution step. Indeed, the dissolution process is triggered manually after the dissolution stick has been connected to the sample. The timing is very critical as the sample starts to warm up, which we believe leads to strong solid-state paramagnetic relaxation of the ^{1}H spins.[13] The polarization with field inversion is larger than without for all molecules, indicating that the field inversion does induce a polarization transfer. The relatively high ^{13}C polarizations without field inversion for ^{13}C-formate and [3-^{13}C]-pyruvate of 2% and 6%, respectively, may be surprising at first sight, in the light of our theoretical predictions. However, our theory only describes the coherent effect of FIRE. The two molecules with strong ^{1}H-^{13}C J couplings also have strong ^{1}H-^{13}C dipolar couplings, which leads to a spontaneous polarization transfer *via* the incoherent cross-relaxation effects.[28,34–36] Note that the T_1 values are significantly longer for the experiment without field inversion.

We repeated the dDNP experiment with field inversion, but monitored the full decay of the ^{1}H polarization after injection with 1° pulses every 1 s. This corresponds to the same experiment as in Fig. 4, but with a field inversion. Figure 5 shows a comparison between the ^{1}H-detected experiments without and with field inversion. The first spectrum was recorded 1 s after injection and is shown in panels A and D, respectively. For the experiment without field inversion, all signals have the same phase, as expected for a standard dDNP experiment without field inversion. The signals of the four ^{13}C-labeled molecules consist of doublets. Those of the three isotopomers of pyruvate are centered around 2.3 ppm. Those of [1-^{13}C]-pyruvate and [2-^{13}C]-pyruvate overlap due to the weak ^{1}H-^{13}C J-couplings (6.2 and 1.3 Hz, respectively), while that of [3-^{13}C]-pyruvate is resolved due to the strong coupling (125 Hz). The group of signals between the water and pyruvate signals probably originate from hyperpolarized residual ^{1}H atoms of glycerol-d_8. The appearance of the spectrum with field inversion is very different; the spectrum is dominated by a strong signal (more than two orders of magnitude stronger than that shown in Fig. 5A) which is the result of "radiofrequency amplification by stimulated emission of radiation" (RASER).[37] This non-linear effect occurs when the current induced in the receiver coil by strong negative magnetization acts as a pulse on the magnetization itself;[38] the fraction of magnetization in the transverse plane induces current in the receiver coil acting like a pulse converting more longitudinal magnetization into transverse magnetization. This results in flipping back the magnetization along the direction of the magnetic field causing characteristic signal bursts in the free induction decay (FID) (see Fig. 5E), much stronger than that induced by the initial 1° pulse without RASER (see Fig. 5B for comparison). The presence of the RASER effect in this experiment shows without doubt that the field inversion has inverted the direction of the magnetization with respect to the magnetic field, at least for some of the spins.

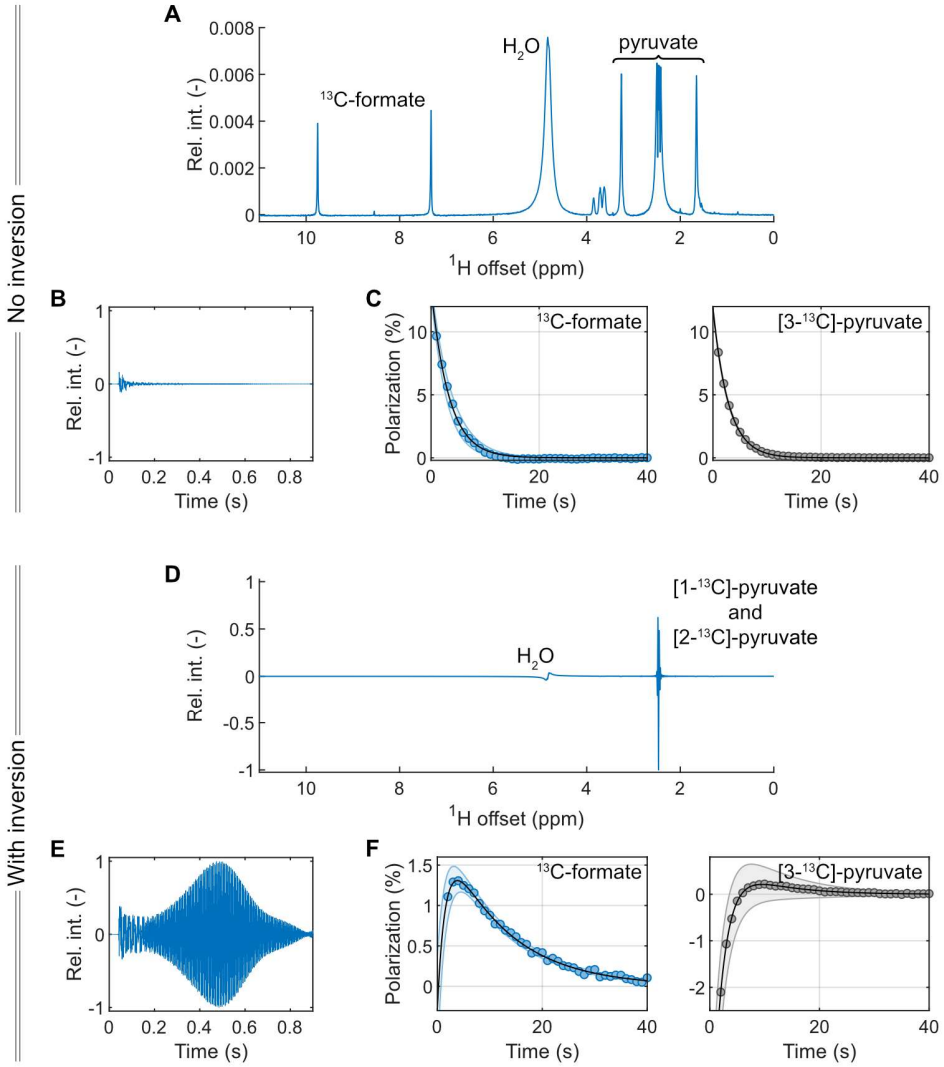

Figure 6: First hyperpolarized ^{1}H spectra (A, D) recorded 1 s after injection using a 1° pulse, corresponding FIDs (B, E), and polarization as a function of time for ^{13}C-formate and [3-^{13}C]-pyruvate (C, F), without and with field inversion during the transfer, respectively. The spectra and their respective FIDs are expressed using the same scale for the *y*-axis, which is normalized with respect to the intensity of the signals in panels D and E. The experimental data in panels C and F (colored dots) are fitted with a mono-exponential decay and bi-exponential function decaying to 0, respectively (black lines). The colored areas around the fitted curves represent the predicted polarization with 95% confidence.

Two groups of resonances contribute to the RASER, the singlet of water and the two doublets of [1-^{13}C]-pyruvate and [2-^{13}C]-pyruvate (see Fig. 5B). This polychromatic RASER makes the interpretation of the phases of the peaks complicated. Yet, this does not affect the most relevant peaks, *i.e.*, those of ^{13}C-formate and [3-^{13}C]-pyruvate. Note that the RASER is only present in the first spectrum of the decay. Its only consequence for the subsequent signal acquisition is that it flipped the water magnetization along the magnetic field in the beginning of the decay. Figs. 5C and F show the time evolution of the polarization of ^{13}C-formate and [3-^{13}C]-pyruvate without and with field inversion, respectively. Polarizations decay monotonically for the experiment without field inversion. On the contrary, they increase until a maximum and only then decay towards 0, in the case of the experiment with field inversion. Polarizations over time were fitted with mono-exponential and bi-exponential functions in the case of the experiment without and with inversion, respectively. Figs. 5C and F show the fitted

polarizations along time. Table 2 summarizes the time constants of the models and the polarizations extrapolated at the time of injection. Again, T_1 values are longer for the experiment without field inversion.

Table 2: ^{1}H longitudinal relaxation time constants and other time constants in s and polarizations in % at the time of injection obtained by mono-exponential decay or bi-exponential fits of the hyperpolarized signals recorded using 1° pulses. The error bars correspond to error on the fit (which do not include the uncertainty on signal integrals). T_f and T_S are the fast and slow time constants of the bi-exponential model, respectively.

	^{13}C-formate			[3-^{13}C]-pyruvate		
	T_f or T_1(^{1}H)	T_s	P(^{1}H)	T_f or T_1(^{1}H)	T_s	P(^{1}H)
With inversion	1.5 ± 0.4	11.8 ± 0.5	-1.5 ± 1.1	2.05 ± 0.7	8.1 ± 0.6	-9 ±1
No inversion	3.3 ± 0.2	–	16.5 ±1	2.84 ± 0.03	–	15.4 ± 0.2

	[1-^{13}C]-pyruvate and [2-^{13}C]-pyruvate		H_2O	
	T_1(^{1}H)	P(^{1}H)	T_1(^{1}H)	P(^{1}H)
With inversion	2.68 ± 0.03	-7.8 ± 0.1	2.74 ± 0.03	0.79 ± 0.02
No inversion	3.07 ± 0.02	11.61 ± 0.06	4.16 ± 0.03	4.38 ± 0.02

The bi-exponential nature of the ^{1}H signals over time for ^{13}C-formate and [3-^{13}C]-pyruvate after polarization transfer by FIRE may be explained by the nuclear Overhauser effect (NOE).[39] Following FIRE, ^{1}H spins are negatively polarized and relax towards thermal equilibrium within a few seconds (mainly due to paramagnetic relaxation). The negative polarization of ^{13}C spins relaxes slower and can therefore cross-relax onto ^{1}H spins. Since these molecules are small and tumble rapidly in solution, the double-quantum cross-relaxation rate is faster, which causes a sign inversion of the transferred polarization and, hence, the observed positive ^{1}H polarization build-up. Similar observations have been reported by other authors. ^{1}H spins in methyl groups hyperpolarized either by either dDNP[28,40] or quantum rotor-induced polarization (QRIP)[41] have been shown to cross-relax to the methyl ^{13}C. Negroni *et al.* gave a detailed account of the polarization transfer pathways between equivalent ^{1}H spins and a single ^{13}C spin, mediated by dipolar ^{1}H-^{13}C interactions during the transfer of a hyperpolarized solution between the dDNP polarizer and the liquid-state spectrometer.[28] For all molecules where the liquid-state T_1 could be reliably fitted to the polarization decay, we found that the value was longer for the experiment without field inversion. This might be explained by the presence of RASER effects in all experiments with field inversion. Indeed, following RASER, the sample is split into regions of opposite polarization because RASER is only effective in the active volume of the NMR coil. Spins that have been subject to RASER have opposite polarization inside and outside the active volume of the coil. T_1 measurements are therefore likely to be influenced by diffusion of molecules between the sample regions inside and outside the active volume of the NMR coil. Even if molecules are not directly subject to RASER, this putative mechanism may still affect them *via* an intermolecular NOE between ^{1}H spins.[7–9] A detailed analysis of these effects is beyond the scope of the present work.

The ^{1}H polarization decay in the liquid-state without field inversion allowed us to extrapolate the polarizations of ^{13}C-formate and [3-^{13}C]-pyruvate at the moment of the field inversion, *i.e.*, ~0.7 s before injection. We found that the ^{1}H polarizations were 16.5% ± 1% and 15.4% ± 0.2%, respectively. From these numbers, Eqs. 4 and 5 (for ^{13}C-formate and [3-^{13}C]-pyruvate, respectively) give the theoretical ^{1}H and ^{13}C polarizations after FIRE, assuming that the initial ^{13}C polarization was 0 due to the saturation pulses in the solid state before dissolution.

The theoretically-predicted polarization values are compared in Table 3 with the experimentally-measured values extrapolated from the measurements with field inversion. The differences between the theoretical predictions and the experimental values are all within 10% of the experimental values. Note that the ^{1}H polarization after FIRE for ^{13}C-formate is expected to be exactly 0 so the relative difference between theory and experiment was not calculated. The experimental value is close to zero although 0 is not within the 95% confidence interval.

Table 3: Comparison of the experimental ^{1}H and ^{13}C polarizations of ^{13}C-formate and [3-^{13}C]-pyruvate immediately after inversion (extrapolated from the liquid-state decays with field inversion) with the prediction of Eqs. 4 and 5 assuming initial ^{1}H polarizations of 16.5% ± 1% and 15.4% ± 0.2%, respectively, while the ^{13}C polarizations were assumed to be 0 for both molecules (the initial ^{1}H polarization was extrapolated from the decay without field inversion)

	^{13}C-formate			[3-^{13}C]-pyruvate		
	Experimental	Predicted	Relative difference	Experimental	Predicted	Relative difference
$P_f(^{1}H)$ (%)	1.5 ± 1.1	0	-	9.6 ± 1.2	8.9 ± 0.1	0.07 ± 0.4
$P_f(^{13}C)$ (%)	17.6 ± 0.2	16.5 ± 1	0.06 ± 0.2	18.4 ± 0.4	19.1 ± 0.2	0.04 ± 0.1

The agreement between theoretical predictions and experiments results shows that adiabatic field inversion is capable of transferring ^{1}H Zeeman order produced by dDNP to ^{13}C in the liquid state. So far, we showed the applicability of the method for molecules with large *J* couplings. Although we used [1-^{13}C]-pyruvate as a control molecule, for which the transfer did not occur with the chosen experimental parameters, this very molecule is most relevant for *in vivo* imaging. Polarizing [1-^{13}C]-pyruvate with ^{1}H-dDNP followed by FIRE would be experimentally more challenging because the inversion time for an adiabatic transfer is longer for molecules with weaker *J* couplings (see the Theory section). However, the inversion time can be reduced to the minimum using a constant adiabaticity-field profile as proposed by Rodin *et al.*, in the context of singlet NMR and parahydrogen hyperpolarization (PHIP).[30,42] Figure 7A shows the constant-adiabaticity field profile computed iteratively for [1-^{13}C]-pyruvate, starting from +5 μT and ending at –5 μT, following Rodin *et al.*'s method (see the Supplementary Material). Once the magnetic field strength is above the μT range, the *J* interaction becomes small compared with the Zeeman interaction. Hence, a rapid variation of the magnetic field intensity beyond this range still allows the transition to be adiabatic, which explains the asymptotic behavior of the curve in Fig. 7A. The final polarizations of ^{1}H and ^{13}C spins after FIRE was simulated numerically as in Fig. 3D, but this time using the constant-adiabaticity field profile of Fig. 7A, assuming initial polarization of 1 and 0, respectively (see solid lines in Fig. 7B). The simulation shows that the maximum ^{13}C polarization is reached for a field inversion time of ~1 s, while 74% of the maximum ^{13}C polarization is reached after only 0.2 s. These values being non-negligible compared to T_1 of ^{1}H spins, the simulation was repeated including relaxation, using a phenomenological relaxation superoperator,[43] assuming the extreme narrowing limit, that it, that the longitudinal relaxation time

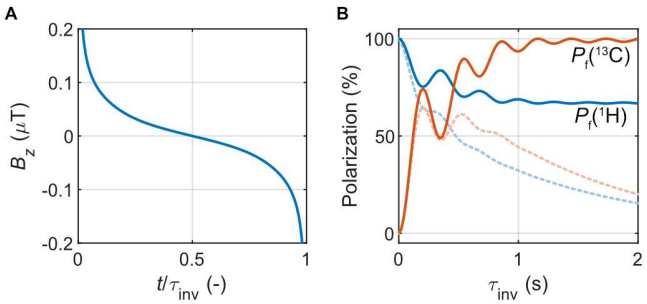

Figure 7: **A**. Constant-adiabaticity field inversion profile for [1-^{13}C]-pyruvate expressed as magnetic field intensity as a function of the relative time along the inversion from +5 μT to –5 μT. **B**. Final ^{1}H and ^{13}C polarizations after field inversion using the constant-adiabaticity profile of panel a, as a function of the inversion time, obtained by numerical simulation assuming initial polarizations of 1 and 0, respectively. The solid and faint dashed lines do not and do include relaxation, respectively.

constant T_1 was equal to the transverse relaxation time constant T_2. It was also assumed that the radicals had been removed from the hyperpolarized solution to avoid paramagnetic relaxation. The exact field dependence of the T_1 for ^{1}H and ^{13}C is complicated to obtain. We therefore used a rough yet conservative estimate that $T_1(^1\text{H}) = T_1(^{13}\text{C})$ all along the transfer and set the value to 5.3 s, which was measured for ^{1}H spins at 1.88 T by inversion recovery for 2.6 M of [1-^{13}C]-pyruvate in D_2O (see Figure S6). The value of $T_1(^{13}\text{C})$ exceeds 100 s in the same conditions. However, ^{1}H and ^{13}C spins are strongly coupled at zero field, which implies that their relaxation rate is governed by the fastest relaxing species, *i.e.*, the ^{1}H spins. The resulting final polarizations are shown by faint lines in Fig. 7B. A ^{13}C polarization of 65% was obtained for the simulation with an inversion time of 0.2 s.

Conclusion and Outlook

We have shown that FIRE is capable of transferring ^{1}H polarization to ^{13}C spins during the transport of a ^{1}H-hyperpolarized solution from the dDNP polarizer to the liquid-state spectrometer, by making the spins experience an adiabatic magnetic field inversion. FIRE makes use of state mixing at zero field due to the heteronuclear J interaction. Our experimental demonstration of FIRE used an in-line magnetic field inversion, realized by commercially-available magnetic shields equipped with solenoid coils on 3D-printed supports. We demonstrated liquid-state ^{13}C polarizations up to 17% that were achieved after only a few minutes of ^{1}H DNP. Spontaneous transfers *via* NOE were also shown to be active, but yielded ^{13}C polarizations 2-10 times lower than FIRE. The detailed analysis of the time evolution of the liquid-state polarizations allowed us to extrapolate the polarizations right before and after field inversion (happening between the dDNP polarizer and the liquid-state spectrometer) and were found to be in agreement with our theoretical predictions.

Although the polarization values we reached are lower than the state of the art ($P(^{13}\text{C}) \approx 50\%$), ^{1}H-dDNP followed by $^1\text{H}\rightarrow^{13}\text{C}$ FIRE has the advantage of relying on simpler instrumentation and shorter buildup times than the existing methods. The method could be further improved by extending ^{1}H relaxation times. First, paramagnetic relaxation[27] can be mitigated in several ways; by using photoinduced radicals[44] that can be quenched before dissolution, by using stable radicals and chemically quenching them during the dissolution process,[45,46] or by using filterable polarizing solids.[47,48] Second, intramolecular dipolar relaxation, which is strong between ^{1}H spins in the methyl moiety, could be reduced by maintaining the sample at a higher temperature throughout the dissolution process.[13]

We provided proof of concept FIRE-dDNP for molecules with large J couplings. Numerical simulations including relaxation showed that the transfer would be possible for [1-^{13}C]-pyruvate, *i.e.*, the most relevant hyperpolarized tracer for *in vivo* imaging. It was found that ~65% of the ^{1}H polarization could be transferred to the ^{13}C spins with an inversion time of ~0.2 s. This could be realized with the in-line approach proposed here. However, an alternative approach where the FIRE is performed while the solution is immobilized could be more efficient. The solution would be collected in a vessel located within magnetic shields (this corresponds to the step where the solution settles down after being pushed by pressurized helium gas in typical dDNP setups[12]). The magnetic field inversion could then be applied by a computer-controlled coil while the solution settles down.[30] The use of computer-controlled coils would be convenient to apply a constant-adiabaticity field inversion profile, therefore minimizing the inversion time and maximizing the transfer efficiency. Hyperpolarization [1-^{13}C]-pyruvate by $^1\text{H}\rightarrow^{13}\text{C}$ FIRE-dDNP would allow one to prepare hyperpolarized tracers for *in vivo* imaging applications in only a few minutes without introducing supplementary demanding or fragile hardware equipment to the dDNP apparatus.

Acknowledgements

We acknowledge *Bruker Biospin* for providing the prototype dDNP polarizer and the Fourier 80, in particular D. Eshchenko, R. Melzi, M. Rossire, M. Sacher, and J. Kempf for scientific and technical support on the dDNP polarizer, and V. Decker, B. Knittel, and F. Decker and for technical support on the Fourier 80 spectrometer. We additionally acknowledge C. Jose and C. Pages for use of the ISA Prototype Service, and S. Martinez of the UCBL mechanical workshop for machining parts of the experimental apparatus. We thank R. Picazo-Frutos and D. Budker for lending us the magnetic shields and S. Lambert for providing advice on coil construction. This research was supported by ENS-Lyon, the French CNRS, Lyon 1 University, the European Research Council

under the European Union's Horizon 2020 research and innovation program (ERC grant agreement no. 714519/HP4all and Marie Skłodowska-Curie grant agreement no. 766402/ZULF).

Author contributions

The idea appeared to S.J. K.I. and S.J. conceived the experiment. K.I., Q.S., Q.R.-F., and S.J.E. developed the numerical simulations. Q.S, Q.R.-F., and S.J.E. optimized the field profile. Q.S. performed the analytical calculations. Q.S., Q.R.-F., and O.C. performed the experiments. Q.S., M.C., and Q.R.-F. conceived the inversion chamber. Q.S. analyzed the data and wrote the manuscript.

Data availability

The experimental data presented in this work can be downloaded at https://doi.org/10.5281/zenodo.8273080. The *MATLAB* scripts used to analyze the experimental data and for all simulations can be downloaded at https://doi.org/10.5281/zenodo.8273380. PDF versions of the codes are available together with the scripts.

Competing interests

The authors declare that they have no competing interests.

References

(1) Eills, J.; Budker, D.; Cavagnero, S.; Chekmenev, E. Y.; Elliott, S. J.; Jannin, S.; Lesage, A.; Matysik, J.; Meersmann, T.; Prisner, T.; Reimer, J. A.; Yang, H.; Koptyug, I. V. *Spin Hyperpolarization in Modern Magnetic Resonance*; preprint; Chemistry, 2022. https://doi.org/10.26434/chemrxiv-2022-p7c9r.

(2) Golman, K.; Zandt, R. in't; Lerche, M.; Pehrson, R.; Ardenkjaer-Larsen, J. H. Metabolic Imaging by Hyperpolarized 13C Magnetic Resonance Imaging for *In Vivo* Tumor Diagnosis. *Cancer Research* **2006**, *66* (22), 10855–10860. https://doi.org/10.1158/0008-5472.CAN-06-2564.

(3) Wang, Z. J.; Ohliger, M. A.; Larson, P. E. Z.; Gordon, J. W.; Bok, R. A.; Slater, J.; Villanueva-Meyer, J. E.; Hess, C. P.; Kurhanewicz, J.; Vigneron, D. B. Hyperpolarized ^{13}C MRI: State of the Art and Future Directions. *Radiology* **2019**, *291* (2), 273–284. https://doi.org/10.1148/radiol.2019182391.

(4) Nelson, S. J.; Kurhanewicz, J.; Vigneron, D. B.; Larson, P. E. Z.; Harzstark, A. L.; Ferrone, M.; van Criekinge, M.; Chang, J. W.; Bok, R.; Park, I.; Reed, G.; Carvajal, L.; Small, E. J.; Munster, P.; Weinberg, V. K.; Ardenkjaer-Larsen, J. H.; Chen, A. P.; Hurd, R. E.; Odegardstuen, L.-I.; Robb, F. J.; Tropp, J.; Murray, J. A. Metabolic Imaging of Patients with Prostate Cancer Using Hyperpolarized [1-^{13}C]Pyruvate. *Sci. Transl. Med.* **2013**, *5* (198). https://doi.org/10.1126/scitranslmed.3006070.

(5) Jannin, S.; Dumez, J.-N.; Giraudeau, P.; Kurzbach, D. Application and Methodology of Dissolution Dynamic Nuclear Polarization in Physical, Chemical and Biological Contexts. *Journal of Magnetic Resonance* **2019**, *305*, 41–50. https://doi.org/10.1016/j.jmr.2019.06.001.

(6) Kim, Y.; Hilty, C. Affinity Screening Using Competitive Binding with Fluorine-19 Hyperpolarized Ligands. *Angew. Chem. Int. Ed.* **2015**, *54* (16), 4941–4944. https://doi.org/10.1002/anie.201411424.

(7) Stern, Q.; Milani, J.; Vuichoud, B.; Bornet, A.; Gossert, A. D.; Bodenhausen, G.; Jannin, S. Hyperpolarized Water to Study Protein–Ligand Interactions. *J. Phys. Chem. Lett.* **2015**, *6* (9), 1674–1678. https://doi.org/10.1021/acs.jpclett.5b00403.

(8) Kurzbach, D.; Canet, E.; Flamm, A. G.; Jhajharia, A.; Weber, E. M. M.; Konrat, R.; Bodenhausen, G. Investigation of Intrinsically Disordered Proteins through Exchange with Hyperpolarized Water. *Angew. Chem. Int. Ed.* **2017**, *56* (1), 389–392. https://doi.org/10.1002/anie.201608903.

(9) Hilty, C.; Kurzbach, D.; Frydman, L. Hyperpolarized Water as Universal Sensitivity Booster in Biomolecular NMR. *Nat Protoc* **2022**, *17* (7), 1621–1657. https://doi.org/10.1038/s41596-022-00693-8.

(10) Kim, Y.; Chen, C.-H.; Hilty, C. Direct Observation of Ru-Alkylidene Forming into Ethylene in Ring-Closing Metathesis from Hyperpolarized ^{1}H NMR. *Chem. Commun.* **2018**, *54* (34), 4333–4336. https://doi.org/10.1039/C7CC08135A.

(11) Hilty, C.; Bowen, S. Applications of Dynamic Nuclear Polarization to the Study of Reactions and Reagents in Organic and Biomolecular Chemistry. *Org. Biomol. Chem.* **2010**, *8* (15), 3361–3365. https://doi.org/10.1039/C004420M.
(12) Ardenkjær-Larsen, J. H.; Fridlund, B.; Gram, A.; Hansson, G.; Hansson, L.; Lerche, M. H.; Servin, R.; Thaning, M.; Golman, K. Increase in Signal-to-Noise Ratio of > 10,000 Times in Liquid-State NMR. *Proc. Natl. Acad. Sci. U.S.A.* **2003**, *100* (18), 10158–10163. https://doi.org/10.1073/pnas.1733835100.
(13) Elliott, S. J.; Stern, Q.; Ceillier, M.; El Daraï, T.; Cousin, S. F.; Cala, O.; Jannin, S. Practical Dissolution Dynamic Nuclear Polarization. *Progress in Nuclear Magnetic Resonance Spectroscopy* **2021**, *126–127*, 59–100. https://doi.org/10.1016/j.pnmrs.2021.04.002.
(14) Ardenkjaer-Larsen, J. H.; Macholl, S.; Jóhannesson, H. Dynamic Nuclear Polarization with Trityls at 1.2 K. *Appl Magn Reson* **2008**, *34* (3–4), 509–522. https://doi.org/10.1007/s00723-008-0134-4.
(15) Ardenkjær-Larsen, J. H.; Bowen, S.; Petersen, J. R.; Rybalko, O.; Vinding, M. S.; Ullisch, M.; Nielsen, N. Chr. Cryogen-free Dissolution Dynamic Nuclear Polarization Polarizer Operating at 3.35 T, 6.70 T, and 10.1 T. *Magn. Reson. Med* **2019**, *81* (3), 2184–2194. https://doi.org/10.1002/mrm.27537.
(16) Bornet, A.; Melzi, R.; Jannin, S.; Bodenhausen, G. Cross Polarization for Dissolution Dynamic Nuclear Polarization Experiments at Readily Accessible Temperatures 1.2 < T < 4.2 K. *Appl Magn Reson* **2012**, *43* (1–2), 107–117. https://doi.org/10.1007/s00723-012-0358-1.
(17) Bornet, A.; Pinon, A.; Jhajharia, A.; Baudin, M.; Ji, X.; Emsley, L.; Bodenhausen, G.; Ardenkjaer-Larsen, J. H.; Jannin, S. Microwave-Gated Dynamic Nuclear Polarization. *Phys. Chem. Chem. Phys.* **2016**, *18* (44), 30530–30535. https://doi.org/10.1039/C6CP05587G.
(18) Elliott, S. J.; Ceillier, M.; Cala, O.; Stern, Q.; Cousin, S. F.; Jannin, S. Simple and Cost-Effective Cross-Polarization Experiments under Dissolution-Dynamic Nuclear Polarization Conditions with a 3D-Printed 1H-13C Background-Free Radiofrequency Coil. *Journal of Magnetic Resonance Open* **2022**, *10–11*, 100033. https://doi.org/10.1016/j.jmro.2022.100033.
(19) Elliott, S. J.; Cousin, S. F.; Chappuis, Q.; Cala, O.; Ceillier, M.; Bornet, A.; Jannin, S. Dipolar Order Mediated ¹H → ¹³C Cross-Polarization for Dissolution-Dynamic Nuclear Polarization. *Magn. Reson.* **2020**, *1* (1), 89–96. https://doi.org/10.5194/mr-1-89-2020.
(20) Elliott, S. J.; Cala, O.; Stern, Q.; Cousin, S. F.; Ceillier, M.; Decker, V.; Jannin, S. Boosting Dissolution-Dynamic Nuclear Polarization by Multiple-Step Dipolar Order Mediated 1H→13C Cross-Polarization. *Journal of Magnetic Resonance Open* **2021**, *8–9*, 100018. https://doi.org/10.1016/j.jmro.2021.100018.
(21) Reineri, F.; Boi, T.; Aime, S. ParaHydrogen Induced Polarization of 13C Carboxylate Resonance in Acetate and Pyruvate. *Nat Commun* **2015**, *6* (1), 5858. https://doi.org/10.1038/ncomms6858.
(22) Goldman, M.; Jóhannesson, H.; Axelsson, O.; Karlsson, M. Hyperpolarization of 13C through Order Transfer from Parahydrogen: A New Contrast Agent for MRI. *Magnetic Resonance Imaging* **2005**, *23* (2), 153–157. https://doi.org/10.1016/j.mri.2004.11.031.
(23) Cavallari, E.; Carrera, C.; Boi, T.; Aime, S.; Reineri, F. Effects of Magnetic Field Cycle on the Polarization Transfer from Parahydrogen to Heteronuclei through Long-Range J-Couplings. *J. Phys. Chem. B* **2015**, *119* (31), 10035–10041. https://doi.org/10.1021/acs.jpcb.5b06222.
(24) Eills, J.; Blanchard, J. W.; Wu, T.; Bengs, C.; Hollenbach, J.; Budker, D.; Levitt, M. H. Polarization Transfer via Field Sweeping in Parahydrogen-Enhanced Nuclear Magnetic Resonance. *The Journal of Chemical Physics* **2019**, *150* (17), 174202. https://doi.org/10.1063/1.5089486.
(25) Lindale, J. R.; Eriksson, S. L.; Tanner, C. P. N.; Warren, W. S. Infinite-Order Perturbative Treatment for Quantum Evolution with Exchange. *Sci. Adv.* **2020**, *6* (32), eabb6874. https://doi.org/10.1126/sciadv.abb6874.
(26) Dagys, L.; Bengs, C.; Levitt, M. H. Low-Frequency Excitation of Singlet–Triplet Transitions. Application to Nuclear Hyperpolarization. *The Journal of Chemical Physics* **2021**, *155* (15), 154201. https://doi.org/10.1063/5.0065863.
(27) Kiryutin, A. S.; Rodin, B. A.; Yurkovskaya, A. V.; Ivanov, K. L.; Kurzbach, D.; Jannin, S.; Guarin, D.; Abergel, D.; Bodenhausen, G. Transport of Hyperpolarized Samples in Dissolution-DNP Experiments. *Phys. Chem. Chem. Phys.* **2019**, *21* (25), 13696–13705. https://doi.org/10.1039/C9CP02600B.
(28) Negroni, M.; Guarin, D.; Che, K.; Epasto, L. M.; Turhan, E.; Selimović, A.; Kozak, F.; Cousin, S.; Abergel, D.; Bodenhausen, G.; Kurzbach, D. Inversion of Hyperpolarized ^{13} C NMR Signals through

Cross-Correlated Cross-Relaxation in Dissolution DNP Experiments. *J. Phys. Chem. B* **2022**, *126* (24), 4599–4610. https://doi.org/10.1021/acs.jpcb.2c03375.
(29) Ivanov, K. L.; Pravdivtsev, A. N.; Yurkovskaya, A. V.; Vieth, H.-M.; Kaptein, R. The Role of Level Anti-Crossings in Nuclear Spin Hyperpolarization. *Progress in Nuclear Magnetic Resonance Spectroscopy* **2014**, *81*, 1–36. https://doi.org/10.1016/j.pnmrs.2014.06.001.
(30) Rodin, B. A.; Eills, J.; Picazo-Frutos, R.; Sheberstov, K. F.; Budker, D.; Ivanov, K. L. Constant-Adiabaticity Ultralow Magnetic Field Manipulations of Parahydrogen-Induced Polarization: Application to an AA'X Spin System. *Phys. Chem. Chem. Phys.* **2021**, *23* (12), 7125–7134. https://doi.org/10.1039/D0CP06581A.
(31) Wittig, C. The Landau−Zener Formula. *J. Phys. Chem. B* **2005**, *109* (17), 8428–8430. https://doi.org/10.1021/jp040627u.
(32) Stern, Q.; Cousin, S. F.; Mentink-Vigier, F.; Pinon, A. C.; Elliott, S. J.; Cala, O.; Jannin, S. Direct Observation of Hyperpolarization Breaking through the Spin Diffusion Barrier. *Sci. Adv.* **2021**, *7* (18), eabf5735. https://doi.org/10.1126/sciadv.abf5735.
(33) Ceillier, M.; Cala, O.; El Daraï, T.; Cousin, S. F.; Stern, Q.; Guibert, S.; Elliott, S. J.; Bornet, A.; Vuichoud, B.; Milani, J.; Pages, C.; Eshchenko, D.; Kempf, J. G.; Jose, C.; Lambert, S. A.; Jannin, S. An Automated System for Fast Transfer and Injection of Hyperpolarized Solutions. *Journal of Magnetic Resonance Open* **2021**, *8–9*, 100017. https://doi.org/10.1016/j.jmro.2021.100017.
(34) Merritt, M. E.; Harrison, C.; Mander, W.; Malloy, C. R.; Dean Sherry, A. Dipolar Cross-Relaxation Modulates Signal Amplitudes in the 1H NMR Spectrum of Hyperpolarized [13C]Formate. *Journal of Magnetic Resonance* **2007**, *189* (2), 280–285. https://doi.org/10.1016/j.jmr.2007.09.011.
(35) Donovan, K. J.; Lupulescu, A.; Frydman, L. Heteronuclear Cross-Relaxation Effects in the NMR Spectroscopy of Hyperpolarized Targets. *ChemPhysChem* **2014**, *15* (3), 436–443. https://doi.org/10.1002/cphc.201300857.
(36) Donovan, K. J.; Frydman, L. HyperBIRD: A Sensitivity-Enhanced Approach to Collecting Homonuclear-Decoupled Proton NMR Spectra. *Angew. Chem. Int. Ed.* **2014**, n/a-n/a. https://doi.org/10.1002/anie.201407869.
(37) Suefke, M.; Lehmkuhl, S.; Liebisch, A.; Blümich, B.; Appelt, S. Para-Hydrogen Raser Delivers Sub-Millihertz Resolution in Nuclear Magnetic Resonance. *Nature Phys* **2017**, *13* (6), 568–572. https://doi.org/10.1038/nphys4076.
(38) Krishnan, V. V.; Murali, N. Radiation Damping in Modern NMR Experiments: Progress and Challenges. *Progress in Nuclear Magnetic Resonance Spectroscopy* **2013**, *68*, 41–57. https://doi.org/10.1016/j.pnmrs.2012.06.001.
(39) Alonso-Valdesueiro, J.; Elliott, S. J.; Bengs, C.; Meier, B.; Levitt, M. H. Testing Signal Enhancement Mechanisms in the Dissolution NMR of Acetone. *Journal of Magnetic Resonance* **2018**, *286*, 158–162. https://doi.org/10.1016/j.jmr.2017.12.009.
(40) Dumez, J.-N.; Vuichoud, B.; Mammoli, D.; Bornet, A.; Pinon, A. C.; Stevanato, G.; Meier, B.; Bodenhausen, G.; Jannin, S.; Levitt, M. H. Dynamic Nuclear Polarization of Long-Lived Nuclear Spin States in Methyl Groups. *J. Phys. Chem. Lett.* **2017**, *8* (15), 3549–3555. https://doi.org/10.1021/acs.jpclett.7b01512.
(41) Meier, B. Quantum-rotor-induced Polarization. *Magnetic Resonance in Chemistry* **2018**, *56* (7), 610–618. https://doi.org/10.1002/mrc.4725.
(42) Rodin, B. A.; Kozinenko, V. P.; Kiryutin, A. S.; Yurkovskaya, A. V.; Eills, J.; Ivanov, K. L. Constant-Adiabaticity Pulse Schemes for Manipulating Singlet Order in 3-Spin Systems with Weak Magnetic Non-Equivalence. *Journal of Magnetic Resonance* **2021**, *327*, 106978. https://doi.org/10.1016/j.jmr.2021.106978.
(43) Elliott, S. J.; Bengs, C.; Brown, L. J.; Hill-Cousins, J. T.; O'Leary, D. J.; Pileio, G.; Levitt, M. H. Nuclear Singlet Relaxation by Scalar Relaxation of the Second Kind in the Slow-Fluctuation Regime. *The Journal of Chemical Physics* **2019**, *150* (6), 064315. https://doi.org/10.1063/1.5074199.
(44) Pinon, A. C.; Capozzi, A.; Ardenkjær-Larsen, J. H. Hyperpolarized Water through Dissolution Dynamic Nuclear Polarization with UV-Generated Radicals. *Commun Chem* **2020**, *3* (1), 57. https://doi.org/10.1038/s42004-020-0301-6.

(45) Miéville, P.; Ahuja, P.; Sarkar, R.; Jannin, S.; Vasos, P. R.; Gerber-Lemaire, S.; Mishkovsky, M.; Comment, A.; Gruetter, R.; Ouari, O.; Tordo, P.; Bodenhausen, G. Scavenging Free Radicals To Preserve Enhancement and Extend Relaxation Times in NMR Using Dynamic Nuclear Polarization. *Angewandte Chemie International Edition* **2010**, *49* (35), 6182–6185. https://doi.org/10.1002/anie.201000934.
(46) Negroni, M.; Turhan, E.; Kress, T.; Ceillier, M.; Jannin, S.; Kurzbach, D. Frémy's Salt as a Low-Persistence Hyperpolarization Agent: Efficient Dynamic Nuclear Polarization Plus Rapid Radical Scavenging. *J. Am. Chem. Soc.* **2022**, jacs.2c07960. https://doi.org/10.1021/jacs.2c07960.
(47) Cavaillès, M.; Bornet, A.; Jaurand, X.; Vuichoud, B.; Baudouin, D.; Baudin, M.; Veyre, L.; Bodenhausen, G.; Dumez, J.-N.; Jannin, S.; Copéret, C.; Thieuleux, C. Tailored Microstructured Hyperpolarizing Matrices for Optimal Magnetic Resonance Imaging. *Angew. Chem.* **2018**, *130* (25), 7575–7579. https://doi.org/10.1002/ange.201801009.
(48) El Daraï, T.; Cousin, S. F.; Stern, Q.; Ceillier, M.; Kempf, J.; Eshchenko, D.; Melzi, R.; Schnell, M.; Gremillard, L.; Bornet, A.; Milani, J.; Vuichoud, B.; Cala, O.; Montarnal, D.; Jannin, S. Porous Functionalized Polymers Enable Generating and Transporting Hyperpolarized Mixtures of Metabolites. *Nat Commun* **2021**, *12* (1), 4695. https://doi.org/10.1038/s41467-021-24279-2.